0026-895X/07/7202-259–268$20.00
MOLECULAR PHARMACOLOGY
Vol. 72, No. 2
35840/3227164
Mol Pharmacol 72:259–268, 2007
Printed in U.S.A.

APETx1 from Sea Anemone *Anthopleura elegantissima* Is a Gating Modifier Peptide Toxin of the Human *Ether-a-go-go*-Related Potassium Channel[S]

M. Zhang, X.-S. Liu, S. Diochot, M. Lazdunski, and G.-N. Tseng

Department of Physiology, Medical College of Virginia, Virginia Commonwealth University, Richmond, Virginia (M.Z., X.S.L., G.N.T.); and Institut de Pharmacologie Moleculaire et Cellulaire, Centre National de la Recherche Scientifique Unité Mixte de Recherche 6097, Valbonne, France (S.D., M.L.)

Received March 6, 2007; accepted April 30, 2007

ABSTRACT

We studied the mechanism of action and the binding site of APETx1, a peptide toxin purified from sea anemone, on the human *ether-a-go-go*-related gene (hERG) channel. Similar to the effects of gating modifier toxins (hanatoxin and SGTx) on the voltage-gated potassium (Kv) 2.1 channel, APETx1 shifts the voltage-dependence of hERG activation in the positive direction and suppresses its current amplitudes elicited by strong depolarizing pulses that maximally activate the channels. The APETx1 binding site is distinctly different from that of a pore-blocking peptide toxin, BeKm-1. Mutations in the S3b region of hERG have dramatic impact on the responsiveness to APETx1: G514C potentiates whereas E518C abolishes the APETx1 effect. Restoring the negative charge at position 518 (methanethiosulfonate ethylsulfonate modification of 518C) partially restores APETx1 responsiveness, supporting an electrostatic interaction between E518 and APETx1. Among the three hERG isoforms, hERG1 and hERG3 are equally responsive to APETx1, whereas hERG2 is insensitive. The key feature seems to be an arginine residue uniquely present at the 514-equivalent position in hERG2, where the other two isoforms possess a glycine. Our data show that APETx1 is a gating modifier toxin of the hERG channel, and its binding site shares characteristics with those of gating modifier toxin binding sites on other Kv channels.

Except for a few recent cases, membrane channels have not been amenable to direct structural determination by crystallography. Peptide toxins targeting ion channels have been used to probe the conformations of their binding sites on the target channels in a so-called "peptide toxin footprinting" approach (Goldstein et al., 1994; Aiyar et al., 1995; Hidalgo and MacKinnon, 1995; Ranganathan et al., 1996; Imredy and MacKinnon, 2000). This information can help us understand the structural basis for toxin-channel interactions and, importantly, can be useful in designing channel-specific modulators as therapeutic agents (Rauer et al., 2000).

A voltage-gated potassium (Kv) channel encoded by the human *ether-a-go-go*-related gene (hERG) is expressed in cardiac myocytes and several other cell types (Sanguinetti et al., 1995; Zhou et al., 1998; Rosati et al., 2000; Bauer et al., 2003). Currents through the hERG channels in cardiac myocytes (rapid delayed rectifier current; I_{Kr}) (Sanguinetti et al., 1995) are important for electrical stability of the heart (Tseng, 2001). There has been a strong interest in the structure-function relationship of the hERG channel, fueled by the need of pharmaceutical industry to predict chemical structures that may lead to hERG/I_{Kr} suppression, which can be potentially linked to the acquired long QT syndrome (Hoffmann and Warner, 2006). Peptide toxins targeting the hERG channel are useful tools in this line of research.

Several such peptide toxins have been identified (Gurrola et al., 1999; Korolkova et al., 2001; Corona et al., 2002; Nastainczyk et al., 2002; Huys et al., 2004). Two peptide toxins purified from scorpions, BeKm-1 and CnErg1 (also called ErgTx1), are the best-studied cases (Korolkova et al., 2002; Pardo-López et al., 2002a,b; Zhang et al., 2003; Tseng et al., 2007). Both toxins bind to hERG's outer vestibule to

This study was supported in part by grant R01-HL46451 from the National Heart, Lung and Blood Institute, National Institutes of Health (to G.N.T.), and in part by a Beginning Grant-in-Aid award from American Heart Association/Mid-Atlantic Affiliate (to M.Z.).

Article, publication date, and citation information can be found at http://molpharm.aspetjournals.org.

doi:10.1124/mol.107.035840.

[S] The online version of this article (available at http://molpharm.aspetjournals.org) contains supplemental material.

ABBREVIATIONS: Kv, voltage-gated potassium; hERG, human *ether-a-go-go*-related gene; $V_{0.5}$, half-maximum activation voltage; z_g, equivalent gating charge; I_C, control current; I_{Tx}, current in the presence of toxin; S3b, carboxyl half of Ser3 segment; MTSES, methanethiosulfonate ethylsulfonate; MTSET, methanethiosulfonate ethyltrimethylammonium; STX, saxitoxin; ANOVA, analysis of variance; WT, wild type; DTT, dithiothreitol; PDB, Protein Data Bank; MTS, 3-(4,5-dimethylthiazol-2-yl)-2,5-diphenyl tetrazolium bromide.

suppress ion conduction through the pore. Their backbone fold consists of an α-helix and a triple-stranded antiparallel β-sheet (PDB identification numbers 1J5J and 1PX9, respectively) (Korolkova et al., 2002; Frenál et al., 2004). An alanine-scanning mutagenesis study showed that BeKm-1 uses its α-helix and the following turn as the interaction surface in binding to the hERG channel (Fig. 1A) (Korolkova et al., 2002). BeKm-1 does not totally occlude ion flux through the hERG pore (Zhang et al., 2003), probably because it binds above the selectivity filter (Tseng et al., 2007).

APETx1 is a new peptide toxin purified from sea anemone (Diochot et al., 2003). Its solution structure has been solved by NMR (Fig. 1B; PDB identification number 1WQK) (Chagot et al., 2005). APETx1 targets the hERG channel, but it differs from BeKm-1 and CnErg1 in two aspects. First, it has an all β-strand folding pattern, distinctly different from that of BeKm-1 or CnErg1 (Fig. 1). Second, although BeKm-1 and CnErg1 suppress not only hERG (isoform 1) but also its two isoforms (hERG2 and hERG3), APETx1 seems to be specific for hERG isoform 1 (Restano-Cassulini et al., 2006). A structural analysis suggests that positive charges along with neighboring aromatic/hydrophobic residues (Lys8 with Tyr5, and Lys18 with Tyr32/Phe33) may be involved in APETx1 binding to the hERG channel (Chagot et al., 2005). The spatial relationship among Lys18, Tyr32, Phe33, and Leu34 on APETx1 bears some resemblance to the relationship among residues on BeKm-1 that are involved in binding to the hERG channel (Lys18, Phe14, and Tyr11) (Fig. 1) (Korolkova et al., 2002; Tseng et al., 2007). However, the mechanism of APETx1's action and its binding site on the hERG channel have not been investigated. This study is designed to tackle these issues and to compare APETx1 effects on the three hERG isoforms. We also discuss the implications of our findings in terms of movement of the gating-paddle during activation of the hERG channel.

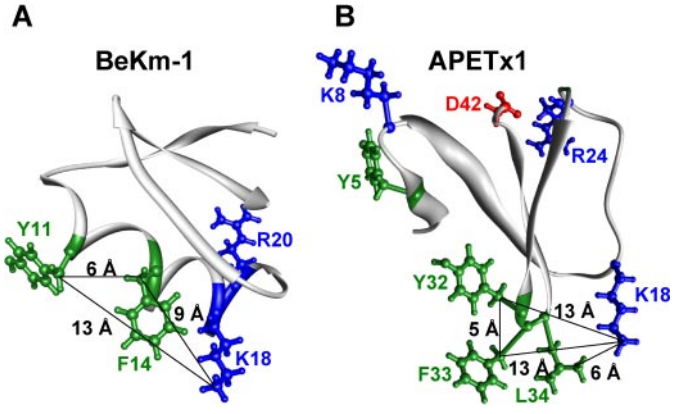

Fig. 1. Comparison of structures of BeKm-1 (PDB identification number 1J5J) (A) and APETx1 (1WQK) (B). BeKm-1 residues that have been shown to interact with residues on the outer vestibule of hERG (Fig. 3A) (Tseng et al., 2007) are highlighted in stick-and-ball format: Lys18, Arg20, Tyr11, and Phe14. The following distances are marked: Lys18 (N_ε) to Phe14 (C_β), 9 Å; Lys18 (N_ε) to Tyr11 (C_β), 13 Å; and Phe14 (C_β) to Tyr11 (C_β), 6 Å. For APETx1, positively or negatively charged residues and several aromatic or hydrophobic residues are highlighted in ball-and-stick format. The following distances are marked: Lys18 (N_ε) to Phe33 (C_β), 13 Å; Lys18 (N_ε) to Tyr32 (C_β), 13 Å; Phe33 (C_β) to Tyr32 (C_β), 5 Å; and Lys18 (N_ε) to Leu34 (C_δ), 6 Å.

Materials and Methods

Toxin Preparation. APETx1 was purified as described before (Diochot et al., 2003). In brief, a crude water-methanol extract of sea anemone *Anthopleura elegantissima* was purified by anion exchange chromatography (QAE Sephadex A-25, 45 × 400 mm, eluted with ammonium acetate, pH 8.3) followed by two runs of gel filtration (Sephadex G50 in 1 M acetic acid). The major peak was lyophilized, dissolved in 0.1% trifluoroacetic acid at 1 mg/ml, and purified by reverse-phase high-performance liquid chromatography (Beckman ODS C18 column, 10 × 250 mm; Beckman Coulter, Fullerton, CA). A linear gradient from 10 to 40% of 0.1% trifluoroacetic acid in acetonitrile was set up at a flow rate of 1 ml/min in 30 min. Fractions of interest were further purified on a cation exchange column TSK-SP 5PW (7.5 × 75 mm; Toyosoda, Tokyo, Japan) with a linear gradient from 0 to 100% of 1 M ammonium acetate in 50 min. Final purification of the major peak was carried out using the same reverse-phase high-performance liquid chromatography as described above. Recombinant BeKm-1 was purchased from Alomone Labs (Jerusalem, Israel).

Cysteine Scanning Mutagenesis and cRNA Transcription. The hERG (isoform 1) was a kind gift from Dr. Gail A. Robertson (University of Wisconsin, Madison, WI). It was subcloned into a vector, pAlterMax, to produce cysteine mutants using an oligonucleotide-directed method (Altered Site Mammalian Mutagenesis System; Promega, Madison, WI). Residues in the outer vestibule region and the S3b region were substituted by cysteine one at a time. Mutations were confirmed by direct DNA sequencing. The mutants are designated by the wild-type (WT) residue (one letter code), followed by position number and "C" for cysteine. The hERG isoforms 2 and 3 were a kind gift from Dr. Barry Ganetzky (University of Wisconsin). In vitro transcription of cDNA was done using a commercial kit (mMessage mMachine; Ambion, Austin, TX). The quality and quantity of cRNA products were analyzed by densitometry (ChemiImager model 4000; Alpha Innotech, San Leandro, CA) using a known amount of RNA size markers as reference.

Oocyte Preparations. Stage V oocytes were isolated from *Xenopus laevis* frogs (Xenopus One) and freed from follicular cell layers after mild collagenase treatment. Each oocyte was injected with 40 nl of solution containing 10 to 18 ng of cRNA. Oocytes were incubated in an ND96-based medium (96 mM NaCl, 2 mM KCl, 1.8 mM $CaCl_2$, 1 mM $MgCl_2$, 5 mM HEPES, and 2.5 mM sodium pyruvate, pH 7.5) supplemented with horse serum (4%) and antibiotics (penicillin 50 U/ml and streptomycin 50 U/ml) at 16°C for 2 to 4 days before voltage-clamp recordings.

Voltage Clamp Experiments. Voltage clamp was done with the two-microelectrode method using an Oocyte Clamp amplifier (model 725B or 725C; Warner Instruments, Hamden, CT). Voltage-clamp protocol generation and data acquisition were controlled by pClamp 5.5 via a 12-bit D/A and A/D converter (Molecular Devices, Sunnyvale, CA). Oocytes expressing cysteine-substituted mutant channels were incubated in DTT-containing medium (10 mM, ≥15 min, room temperature) to reduce disulfide bonds that might have formed spontaneously (Liu et al., 2002). All cysteine-substituted mutant channels examined in this study manifested WT-like properties after DTT treatment (Figs. 3–6). Oocytes were then thoroughly rinsed in DTT-free medium (to avoid reduction of APETx1 by residual DTT) before voltage-clamp recording. The oocyte was placed in a tissue bath containing 0.8 ml of low-[Cl] bath solution (Cl^- ions in ND96 replaced by methanesulfonate to avoid interference from endogenous Cl^- currents) containing 0.1% bovine serum albumin (to prevent peptide toxin from sticking to tubings and plastic well). The grounding electrodes were filled with 3 M KCl (in contact with Ag/AgCl pellets) and connected to the bath solution with salt bridges made of 1% agar in the same low-[Cl] ND96 bath solution. After confirming the stability of membrane currents under the control conditions, voltage-clamp protocols designed to construct the activation curve and fully activated current-voltage ($I_{f\text{-}a}$-V) relationship (described in

the figure legends) were executed. The membrane voltage was then held at −80 mV (V_h, unless otherwise noted), and currents were activated by 1-s test pulses applied once per 120 s to a voltage corresponding to the half-maximum activation voltage of the channel under study. This low level of channel activation facilitated the monitoring of APETx1 effect on the channel (Fig. 2). A suitable amount of APETx1 stock solution was diluted with 0.2 ml of bath solution and added to the bath to reach the desired toxin concentration. The bath solution was pipetted repetitively to facilitate equilibration of toxin concentration in the bath, whereas the progression of toxin effect on the channels was monitored by changes in current amplitude elicited by the above pulse protocol. The pulse protocols for activation curve and $I_{f\text{-}a}$-V relationship were executed after the effect of APETx1 reached a steady state.

The toxin concentrations in experiments reported here ranged from 10 to 10,000 nM. The APETx1 stock solutions were made in 0.1% bovine serum albumin in low-[Cl] ND96 at 10 or 200 μM. To determine the concentration-response relationship, the beginning APETx1 concentration in the bath solution was 10 nM (1000-fold dilution from a 10 μM stock) and was increased cumulatively after the steady-state effect was reached at each concentration.

Data Analysis and Molecular Modeling. Data analysis was performed using the following programs: Clampfit of pClamp 6 or 8 (Axon Instruments), Excel (Microsoft, Redmond, WA), PeakFit, SigmaPlot, and SigmaStat (Systat Software, Inc., Point Richmond, CA). Multiple-group comparison was done using one-way ANOVA followed by Dunn's test against wild-type hERG or Tukey's test of all pair-wise comparisons. Homology modeling of hERG's S3b-S4 based on the corresponding region in the crystal structure of isolated voltage-sensing domain of KvAP (PDB identification number 1ORS) was done using Discovery Studio version 1.6 (Accelrys, San Diego, CA). Distance measurement between toxin side chains was done using the Swiss-pdb Viewer (http://www.expasy.org/spdbv/) (Guex and Peitsch, 1997). Molecular graphics images were produced using the UCSF Chimera package from the Resource for Biocomputing, Visualization, and Informatics at the University of California, San Francisco (San Francisco, CA; supported by National Institutes of Health grant P41-RR01081; http://www.dgl.ucsf.edu/chimera) (Pettersen et al., 2004).

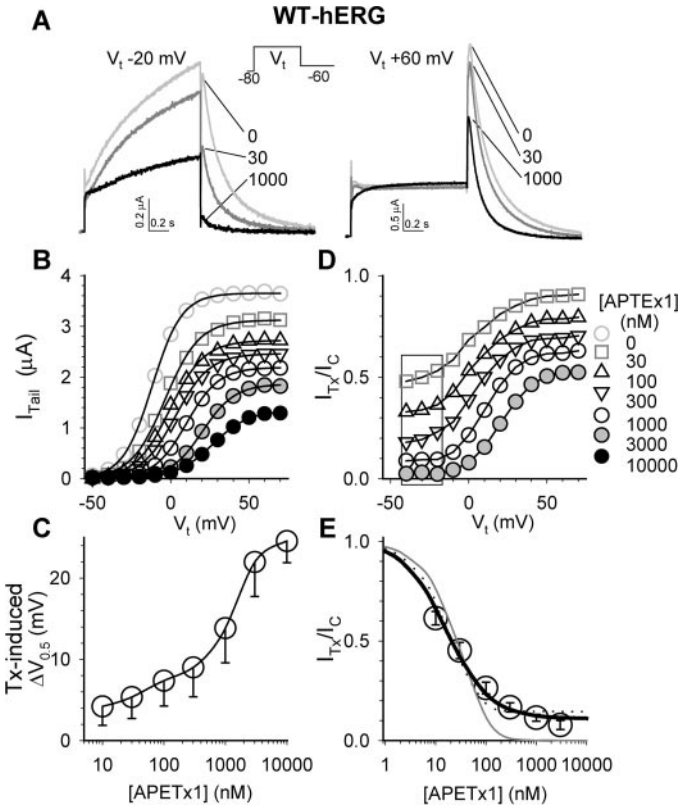

Fig. 2. Concentration-dependent effects of APETx1 on the WT hERG channel. A, current traces elicited by the voltage-clamp protocol diagrammed on top before and after adding APETx1 (30 and 1000 nM). Two test pulse voltages (V_t) are used to show that APETx1 is more potent in suppressing WT-hERG at weak depolarization than at strong depolarization. B, peak amplitudes of tail currents (I_{tail}) recorded before and after adding APETx1 (symbols for different toxin concentrations are listed on the right) are plotted against V_t. The relationship between V_t and I_{tail} is fit with a simple Boltzmann function: $I_{tail} = I_{max}/(1 + \exp[z_g F(V_{0.5} - V_t)/RT])$, where I_{max}, z_g, $V_{0.5}$, F, R, and T are maximum peak tail current amplitude, equivalent gating charge of activation, half-maximum activation voltage, Faraday constant, gas constant, and absolute temperature, respectively. The superimposed curves are calculated from the Boltzmann function. C, degree of shift in $V_{0.5}$ of activation by different concentrations of APETx1 (n = 4–10 each). D, fraction of uninhibited current (I_{Tx}/I_C,) in the presence of different concentrations of APETx1 (same symbols as in B) are plotted against V_t. Boxed area indicates data points (V_t −40 to −20 mV) used to construct the concentration-response relationship shown in E. E, concentration-response relationship quantified by I_{Tx}/I_C values at V_t −40 to −20 mV (n = 4–7 each). Data are fit with three models: 1) four equivalent and independent binding sites per channel with dissociation constant K_d and fractional toxin-sensitive current (A_{max}), $I_{Tx}/I_C = A_{max}[K_d/(K_d + [Tx])]^4 + (1 - A_{max})$, shown by black dotted curve with K_d = 87 nM and A_{max} = 0.86; 2) four equivalent and independent binding sites per channel with fully toxin-sensitive current, $I_{Tx}/I_C = [K_d/(K_d + [Tx])]^4$, shown by gray solid curve with K_d = 141.1 nM; and 3) one binding site per channel and fractional toxin-sensitive current, $I_{Tx}/I_C = A_{max}[K_d/(K_d + [Tx])] + (1 - A_{max})$, shown by black thick curve with K_d = 16.3 nM and A_{max} = 0.89.

Results

APETx1 Shifts the Voltage-Dependence of hERG Activation in the Positive Direction in a Concentration-Dependent Manner. Figure 2A illustrates original current traces of the hERG channel recorded before and after the application of 30 or 1000 nM APETx1. The peak amplitudes of tail currents are used to construct the activation curves shown in Fig. 2B. The data are fit with a simple Boltzmann function (Fig. 2, legend) to estimate the half-maximum activation voltage ($V_{0.5}$) and the equivalent gating charge (z_g). The degrees of $V_{0.5}$ shift caused by different concentrations of APETx1 are summarized from 4 to 10 oocytes and shown in Fig. 2C, and the z_g values are summarized in Supplemental Table S1. The effects of APETx1 on hERG are similar to those of hanatoxin and SGTx, two gating modifier toxins, on the Kv2.1 channel (Lee et al., 2003; Wang et al., 2004; Swartz, 2007): it shifts the activation curve of the hERG channel in the positive direction and reduces the current amplitude elicited by strong depolarizing pulses that reach the maximum level of channel activation (V_t to +70 mV). At V_t +60 mV, the test pulse current is less outward than the tail current at −60 mV (Fig. 2A, right). This is due to the fast and voltage-sensitive inactivation process of the hERG channels that shuts down currents at +60 mV. Upon repolarization to −60 mV, fast recovery from inactivation in conjunction with a slow deactivation process allows a resurgence of outward current through the channel pore. APETx1 does not affect the test pulse current at +60 mV, indicating that the toxin does not interfere with the channel's inactivation process, unlike a nonpeptide hERG gating modifier toxin, saxitoxin (Wang et al., 2003).

To estimate the apparent K_d value of APETx1 binding to the hERG channel, we use the method described previously for quantifying hanatoxin or SGTx binding to the Kv2.1

channel (Lee et al., 2003; Wang et al., 2004; Swartz, 2007). Hanatoxin or SGTx binds to the S3b region of Kv2.1 (Li-Smerin and Swartz, 2000; Swartz, 2007). There could be four binding sites per channel, one each on the four subunits. The relationship between toxin concentration and fraction of uninhibited current (I_{Tx}/I_C, where I_{Tx} and I_C are current amplitude in the presence of toxin and the control current, respectively) is fit with a model of four equivalent and independent binding sites per channel. The I_{Tx}/I_C value is measured from currents elicited by weak depolarizing pulses that induce only threshold level of channel activation under the control conditions. The rationale of using "threshold depolarization voltage" is based on the assumption that under these conditions, channels with even one bound toxin molecule will fail to open, and thus the I_{Tx}/I_C reflects the fraction of channels totally free of toxin. This situation is different from when currents are elicited by strong depolarizing pulses that can activate channels with bound toxin molecules (Phillips et al., 2005). In practice, the suitable voltage range for I_{Tx}/I_C measurement is when the degree of current suppression by these gating modifier toxins reaches a "plateau" level (strongest and relatively constant) (Lee et al., 2003; Wang et al., 2004). Figure 2D shows I_{Tx}/I_C values plotted against test pulse voltage from the same experiment as shown in Fig. 2, A and B. The toxin effect is strongest and relatively constant in the V_t range of −40 to −20 mV (boxed area in Fig. 2D). The toxin effect becomes weaker (I_{Tx}/I_C value becomes higher) at more positive V_t. Therefore, we use I_{Tx}/I_C values in the V_t range of −40 to −20 mV to quantify the fractions of toxin-free channels in the presence of different concentrations of APETx1. Mean data averaged from four to seven measurements each are shown in Fig. 2E. Because of variations in the responsiveness to APETx1 among oocytes expressing the wild-type hERG channel, the mean I_{Tx}/I_C value is >0 even at a toxin concentration of 3 μM. As a result, the data are fit poorly with a model of four equivalent and independent binding sites per channel with fully toxin-sensitive current (gray curve in Fig. 2E). The data can be fit reasonably well with a model of 86% toxin-sensitive current with four equivalent and independent binding sites per channel of K_d = 87 nM (black dotted curve in Fig. 2E). However, the data can also be fit equally well with a model of 89% toxin-sensitive current and one binding site per channel of K_d = 16.3 nM (black solid curve in Fig. 2E). Thus, these data do not allow us to unequivocally determine the apparent K_d value for APETx1 binding to the hERG channel. On the other hand, the degree of $V_{0.5}$ shift observed in the presence of 10 μM APETx1 is less variable (Fig. 2C). Therefore, in the following experiments, we use this single high concentration to compare how mutations introduced into different regions of the hERG channel can affect the responsiveness to APETx1.

APETx1 Binding Site on the hERG Channel Is Distinctly Different from that of BeKm-1. Figure 3B shows that BeKm-1 (10 nM) is equally effective in suppressing the hERG current amplitude in the absence or in the presence of a 100-fold higher concentration of APETx1 (1000 nM). In the latter case, APETx1 is effective in modulating the hERG channel, as is evidenced by the marked slowing of channel activation (open arrows in Fig. 3B). These observations suggest that the two peptide toxins modulate the hERG channel independent of each other.

To further test whether there is any overlap between APETx1 and BeKm-1 binding sites on the hERG channel, we examine the effects of mutations in the outer vestibule region of hERG on the responsiveness to APETx1. Cysteine-scanning mutagenesis of hERG's outer vestibule region has shown that Arg582, Ile583, and Tyr597 (at the two ends of a

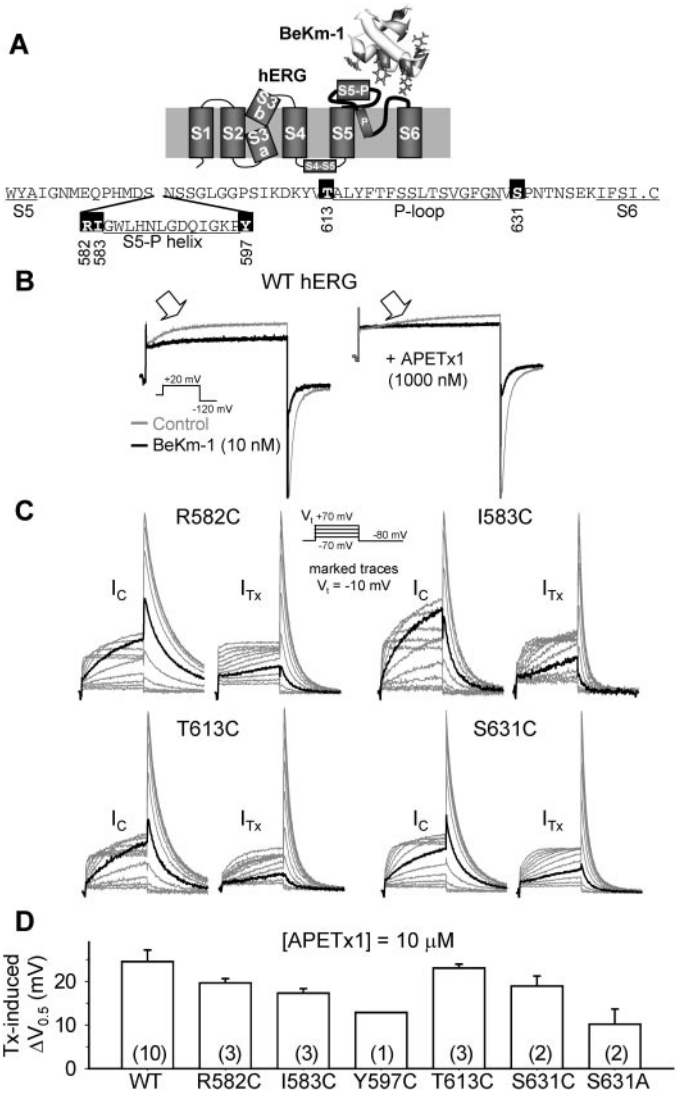

Fig. 3. The APETx1 binding site on hERG is independent of the BeKm-1 binding site. A, top, two-dimensional diagram of an hERG subunit marking the following helices: transmembrane S1 to S6 (S3 divided into S3a and S3b), S5-P (in the S5-P linker), P (in the pore-loop), and S4–S5. An image of BeKm-1 (similar to Fig. 1A) is shown on top of the hERG S5-P and P-S6 linkers that line the outer vestibule. Bottom, hERG amino acid sequence from the end of S5 to the beginning of S6 (underlined). The S5-P helix (as an insert in the S5-P linker) (Jiang et al., 2005) and the P loop are also underlined. Highlighted residues are those interacting with BeKm-1 (Tseng et al., 2007) and are examined here. B, current traces elicited by the diagrammed voltage-clamp protocol before and after adding 10 nM BeKm-1. Currents shown on the right are recorded in the presence of 1000 nM APETx1. Open arrows point to the activation phase of currents. C, four groups of current traces (with mutant types marked on top) recorded before (I_C, left) and after (I_{Tx}, right) adding 10 μM APETx1. The voltage-clamp protocol is diagrammed on top. Current traces are shown in gray, except for those recorded at V_t −10 mV (~half-maximum activation voltage for all four mutant channels under the control conditions) to highlight the toxin-induced change in degree of activation and slowing of activation. D, summary of degree of $V_{0.5}$ shift by 10 μM APETx1. WT and mutant channels are marked along the abscissa; n, number of experiments. One-way ANOVA of multiple groups with $n > 2$, $p = 0.243$.

helix formed in the middle of the S5-P linker, S5-P helix, shown as an insert in Fig. 3A) (Jiang et al., 2005), as well as Thr613 and Ser631 (at the two ends of the pore-loop) are critical for BeKm-1 binding (Zhang et al., 2003). These residues are highlighted by white-lettering on black background in Fig. 3A. Figure 3C depicts original current traces of cysteine-substituted mutant channels recorded before and after the application of 10 μM APETx1. All of the oocytes are DTT-treated to reduce disulfide bonds that may have formed spontaneously (see *Materials and Methods*), which can alter the conformation of hERG's outer vestibule (Liu et al., 2002). With DTT treatment, all of the mutant channels behave like WT hERG in terms of voltage range of activation, degree of inactivation, and K^+ selectivity. Under the control conditions, V_t to -10 mV induces ~50% of maximum activation in these channels (highlighted by black current traces in the I_C panels of Fig. 3C). In all cases, APETx1 10 μM markedly reduces the degree of activation at V_t -10 mV and slows the activation rate (I_{Tx} panels of Fig. 3C). Figure 3D summarizes the degree of $V_{0.5}$ shift caused by 10 μM APETx1. We conclude that there is no overlap between the APETx1 binding site and BeKm-1 binding site on the hERG channel. Because BeKm-1 occupies the central position of the hERG pore domain (Tseng et al., 2007), the APETx1 binding site is likely to be more peripheral, probably in the voltage-sensing domain.

Cysteine Substitution at Two Positions in hERG's S3b Region Has a Marked Impact on APETx1 Effect. Gating modifier toxins bind to the voltage-sensing domains of their target channels to modulate the activation or inactivation process (Cestele et al., 1998; Smith et al., 2005; Swartz, 2007). A "hot spot" for interactions between gating modifier toxins and ion channels is the S3b region (also called the carboxyl half of S3) (Winterfield and Swartz, 2000). We tested the effects of mutations introduced into the S3b region of the hERG channel on the responsiveness to APETx1. Residues at positions 514 to 519 are substituted by cysteine (sequence shown in Fig. 5A). Figure 4 shows the test pulse current-voltage (I-V) relationships and activation curves of these cysteine-substituted mutant channels and compares them with those of WT hERG. All of the mutant channels maintain a strong inactivation process (bell-shaped test pulse I-V, current traces shown in Fig. 5B), and K^+ selectivity (no shift in E_{rev}). Relative to WT hERG, the activation curve of G516C is shifted in the negative direction, whereas those of S517C, E518C, and E519C are shifted in the positive direction. Assuming a two-state (closed and open) gating model, the free energy of channel activation at 0 mV (ΔG_o) is calculated as $z_g V_{0.5} F$ (in kilocalories per mole), where z_g and $V_{0.5}$ are obtained from Boltzmann fit to the activation curve (Fig. 2B legend), and F is the Faraday constant. The shifts in the activation curve shown in Fig. 4 correspond to very modest changes in the ΔG_o value (between -0.29 and 0.95 kcal/mol). Therefore, we conclude that cysteine substitutions per se in the S3b region have only minor effects on the hERG channel function (i.e., the mutations do not cause much perturbation of the native conformation of the channel).

Figure 5B depicts original current traces of the mutant channels recorded before and after the application of 10 μM APETx1. For S515C, G516C, S517C, and E519C, APETx1 slows the rate of activation and reduces the degree of channel activation at V_t values that induce ~50% of maximum activation under the control conditions (black current traces in Fig. 5B). For G514C, V_t of -20 mV induces ~50% of maximum activation under the control conditions but fails to activate the channels in the presence of APETx1. In the presence of APETx1, the threshold for G514C activation is shifted to -10 mV, and the plateau of activation is reached at V_t +120 mV. Pulses to $V_t \geq +80$ mV activate outward currents through oocyte endogenous channels (Fig. 5B, I_{Tx} panel of G514C). These should be followed by small inward tail currents upon repolarization to -80 mV (seen in uninjected oocytes). However, these small inward tail currents are masked by the much larger G514C outward tail current. APETx1 at 10 μM has no discernible effects on the E518C currents. The degrees of $V_{0.5}$ shift caused by 10 μM APETx1 in the S3b mutants are summarized in Fig. 5C. S515C, G516C, S517C, and E519C are as responsive to APETx1 as WT hERG. On the other hand, G514C is more responsive to APETx1 than WT hERG ($V_{0.5}$ shifted by 55.6 $\pm$ 1.3 mV versus 24.6 $\pm$ 2.7 mV in WT hERG, $p < 0.05$), whereas E518C is unresponsive to 10 M APETx1 (shift in $V_{0.5}$ $-0.5 \pm$ 1.0 mV). Position 518 corresponds to position 277 of Kv2.1,

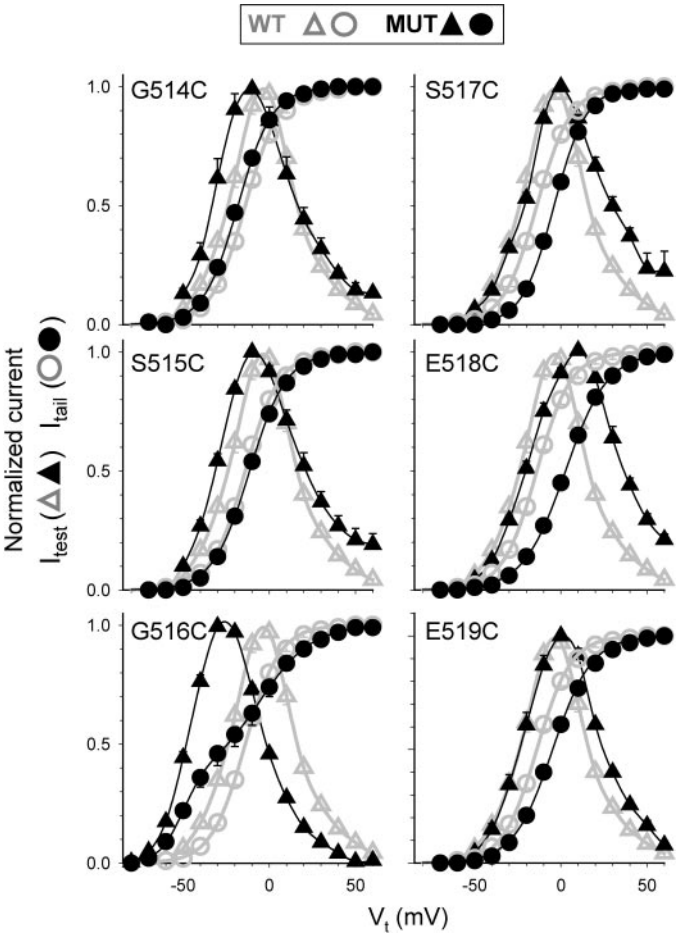

Fig. 4. Characterization of cysteine-substitution mutants in the S3b region of hERG (G514C-E519C). Each panel contains four I-V relationships. The WT data (gray symbols and curves) are the same in all panels. The mutant data are shown as black symbols and curves, with mutant types marked. Triangles denote test pulse currents (I_{test}) normalized to the maximum I_{test} in each cell (occurring at different V_t due to shift in the voltage-range of activation, ranging from -30 mV for G516C to +10 mV for E518C) and averaged over cells. Circles denote I_{tail} normalized by maximum I_{tail} in each cell after V_t to +70 mV and fit with a simple Boltzmann function. Each data point represents the average from 10 to 18 measurements.

whereas position 514 may be equivalent to position 273 or 274 of Kv2.1 (Fig. 5A). These Kv2.1 residues are involved in the binding of hanatoxin and SGTx (Li-Smerin and Swartz, 2000). Therefore, APETx1 is similar to these gating modifier toxins not only in its effects on the hERG channel function but also in its binding site.

It has been shown that the negative charge at position 277 of Kv2.1 is critical for hanatoxin or SGTx binding (Li-Smerin and Swartz, 2000). Preserving the negative charge here (E277D) does not perturb toxin binding, whereas mutating Glu277 to neutral residues causes a 10- to 50-fold increase in K_d value (Li-Smerin and Swartz, 2000). There may be a similar electrostatic interaction between Glu518 of hERG and a positive charge on APETx1, explaining why neutralizing the negative charge at position 518 destroys the responsiveness to APETx1. We tested whether adding back a negative charge to the 518C side chain, by MTSES modification, can restore the APETx1 responsiveness. Treating oocytes expressing E518C with 10 mM MTSES does not induce any detectable changes in the channel function (Fig. 6, A, activation curve, and B, current traces). However, APETx1 10 μM induces a clear positive shift in the voltage-dependence of activation of MTSES-modified E518C channel (Fig. 6, B and C). This supports the notion that a negatively charged side chain at position 518 is needed to stabilize APETx1 binding to hERG. Mutating Glu277 of Kv2.1 to positively charged arginine or lysine causes a >100-fold increase in K_d value (Li-Smerin and Swartz, 2000). To test whether the electrostatic interaction is specific for the side chain at position 518, we add a positive charge to side chain at the flanking positions by reacting 517C or 519C with 1 mM MTSET. Figure 6A shows that MTSET treatment causes a negative shift in the voltage-dependence of activation in S517C and a positive shift in E519C, supporting the effectiveness of MTSET modification of these introduced cysteine side chains (MTSET does not alter the WT hERG channel function) (Fan et al., 1999). However, MTSET modification of 517C or 519C does not alter their responsiveness to APETx1 (Fig. 6, B and C). These data suggest that there is an electrostatic interaction between the S3b of hERG and a positive charge on APETx1, and this interaction is specific for position 518.

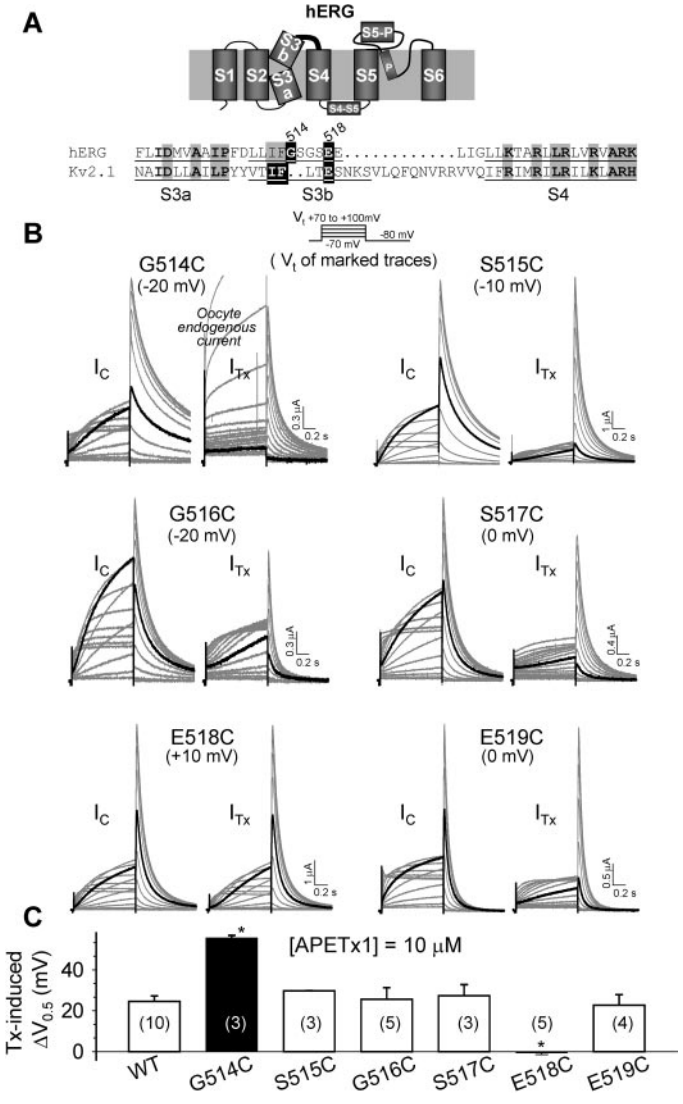

Fig. 5. Cysteine substitution at two positions in hERG's S3b has marked impact on APETx1 effect. A, top, two-dimensional diagram of a hERG subunit as shown in Fig. 3A. Bottom, amino acid sequence alignment of hERG and Kv2.1 from S3a to S4. Identical residues have a gray shade. Gly514 and Glu518 of hERG and Ile273, Phe274, and Glu277 of Kv2.1 are highlighted by white lettering on black background. B, six groups of current traces recorded before (I_C, left) and after (I_{Tx}, right) adding 10 μM APETx1. The format is the same as Fig. 3C, but the V_t value is varied because of $V_{0.5}$ shift caused by the mutations (marked for each mutant type). C, summary of degree of $V_{0.5}$ shift caused by 10 μM APETx1; n, number of measurements. One-way ANOVA, $p = 0.004$; $*$, $p < 0.05$ versus WT.

APETx1 Has Differential Effects on the Three hERG Isoforms. There are two other members in the hERG Kv channel subfamily: hERG2 and hERG3 [hERG is denoted as isoform 1 or hERG(1) in Fig. 7] (Ganetzky et al., 1999). It has been suggested previously that APETx1 is specific for hERG isoform 1 but is ineffective in modulating hERG2 or hERG3 (Restano-Cassulini et al., 2006). Figure 7A shows the amino acid sequence alignment of the three hERG isoforms in the S3b-S4 region. Both hERG2 and hERG3 have three extra threonine residues in their S3b, which are missing in hERG(1). Threonine residue with its hydroxyl side chain tends to destabilize α-helical secondary structures. Therefore, the three threonine residues in hERG2 and hERG3 may perturb the conformation of the S3b helix, disrupting APETx1 binding. On the other hand, hERG2 has a positively charged arginine at the 514-equivalent position (Arg362). Mutating the 514-equivalent residue in Kv2.1 (Phe274, Fig. 5A) to a positively charged residue causes a >500-fold increases in K_d value for hanatoxin binding (Li-Smerin and Swartz, 2000). Therefore the unique positive charge in the S3b of hERG2 may disrupt APETx1 binding. A comparison of APETx1 effects on the three hERG isoforms will reveal which of these features affects toxin binding. Figure 7, B to D, shows that APETx1 up to 1 μM cannot shift the voltage-dependence of activation of hERG2. On the other hand, hERG3 is responsive to APETx1, and there is no statistically significant difference between hERG isoforms 1 and 3 in the degree of $V_{0.5}$ shift caused by 1 μM APETx1 (Fig. 7D). Therefore, the three extra threonine residues in the S3b of hERG2 and hERG3 isoforms do not dominate APETx1 binding. The unique positive charge in the S3b of hERG2 can explain why this channel is insensitive to APETx1.

Discussion

The "Gating Modifier Toxin" Mechanism of APETx1 and Comparison with Other Gating Modifier Toxins. The effects of APETx1 on hERG are similar to those of hanatoxin or SGTx on Kv2.1: it causes a positive shift in the voltage range of activation and decreases the maximum conductance elicited by strong depolarizing pulses to the plateau level of activation. Hanatoxin and SGTx bind to the S3b region of Kv2.1. A negative charge at position 277 in S3b of Kv2.1 is critical, probably by establishing an electrostatic interaction with a positively charged residue on the toxins (Li-Smerin and Swartz, 2000). The equivalent residue on hERG, Glu518, is also important for APETx1 binding. Substituting this glutamate with a neutral cysteine side chain makes the channel insensitive to 10 μM APETx1. MTSES modification of the 518C side chain partially restores the APETx1 sensitivity. This electrostatic interaction between hERG's S3b and APETx1 is specific for position 518: adding a positive charge to 517C or 519C does not reduce APETx1 sensitivity. In Kv2.1, Phe274 and Ile273 are also important for the binding of gating modifier toxins, and this interaction is hydrophobic in nature (Li-Smerin and Swartz 2000). Mutating Ile273 or Phe274 to a charged or hydrophilic residue markedly reduces hanatoxin or SGTx binding. The amino acid alignment suggests that position 514 of hERG is equivalent to position 274 or 273 of Kv2.1. Replacing glycine at position 514 with cysteine increases side chain hydrophobicity. The observed higher responsiveness to APETx1 in G514C supports the notion that a hydrophobic interaction between position 514 and the toxin stabilizes toxin binding. Furthermore, hERG2 differs from hERG1 and hERG3 in having a positive charge (Arg362) at the 514-equivalent position. Previous work on Kv2.1 has shown that introducing a positive charge to position 274 or 273 greatly reduces hanatoxin sensitivity (Li-Smerin and Swartz, 2000). Therefore, the lack of APETx1 responsiveness in hERG2 can be attributed to the unique positive charge in its S3b. We conclude that APETx1 is a gating modifier toxin of the hERG channel. Its binding site is in the S3b region of hERG, which shares characteristics with those of gating modifier toxin binding sites on other Kv channels.

As illustrated in Fig. 2, C and E, we cannot unequivocally quantify the K_d values for APETx1 binding to WT or mutant hERG channels. This may be partly due to technical issues: 1) difficulty in quantifying current amplitudes at threshold depolarizations; 2) use of $V_{0.5}$ value derived from a two-state gating model, which is far from the complexity of voltage-dependence of channel gating; and (3) variations among oocytes in responsiveness to APETx1. However, these factors do not account for a difference of more than an order of magnitude in the apparent EC_{50} values estimated from shifts in $V_{0.5}$ of activation (Fig. 2C) and from reduction in current amplitude (Fig. 2E). More likely, this reflects differences in coupling between toxin binding and the functional parameters measured and perhaps also cooperativity in toxin binding to successive channel subunits.

Saxitoxin (STX) is the only other hERG gating modifier toxin identified so far (Wang et al., 2003). STX is a small molecule carrying two positively charged guanidinium groups. It blocks sodium channel pore from the outside. Its effects on hERG are distinctly different from those on the sodium channel: STX shifts the voltage range of hERG activation in the positive direction, similar to the effect of APETx1. However, STX also interferes with hERG's inactivation process, so that at positive voltages when the degree of inactivation is the dominating factor in determining the current amplitude, STX can actually induce an increase in hERG current amplitude (Wang et al., 2003). Because STX has a much smaller size than APETx1, it can probably penetrate deeper into the water-filled space (crevice) between

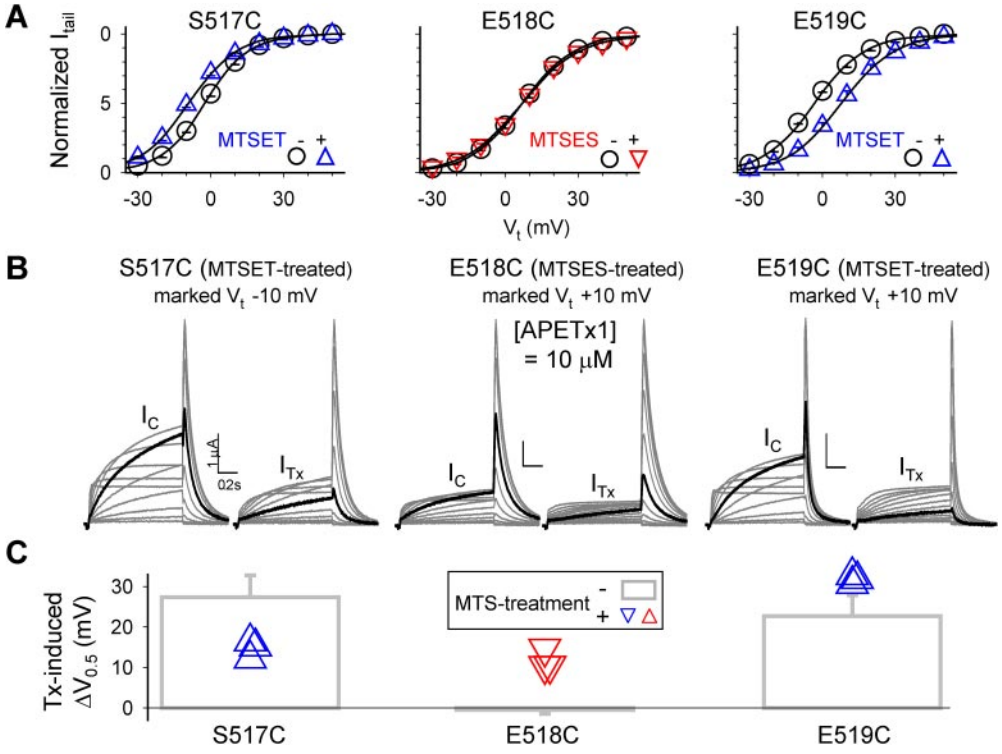

Fig. 6. Effects of thiol-modifying MTS reagents on the S517C, E518C, and E519C mutants of hERG and their response to APETx1. A, voltage-dependence of activation under the control conditions and after MTS treatment (S517C and E519C treated with MTSET and E518C treated with MTSES. n = 3–4 each). B, three groups of current traces recorded from MTSET-treated S571C and E519C and MTSES-treated E518C. I_C and I_{Tx} are currents before and after adding 10 μM APETx1. The voltage-clamp protocol is similar to that diagrammed in Fig. 5, with V_t values shifted −10 mV for S517C and +10 mV for E519C because of MTSET-induced $V_{0.5}$ shift. C, degree of $V_{0.5}$ shift caused by 10 μM APETx1 in MTSET-treated S571C and E519C (blue triangles) and MTSES-treated E518C (red inverted triangles); n = 3 - 4 each. The gray open histogram bars are values of $V_{0.5}$ shift in control (no MTS treatment) oocytes taken from Fig. 5C for comparison. The p values for degrees of $V_{0.5}$ shift between untreated and MTS-treated conditions are 0.083 (S517C), <0.001 (E518C), and 0.40 (E519C).

transmembrane helices in hERG's voltage-sensing domain and influence both activation and inactivation. The STX binding site on the hERG channel has not been identified.

The APETx1 Binding Site on the hERG Channel. The amino acid sequence of hERG's S3b-S4 region is highly homologous to that of KvAP (Fig. 8A, top). This suggests a tight "gating-paddle" structure (helix-turn-helix) in hERG as in KvAP (Fig. 8A, bottom). Positions 518 and 514 are on the same face of the S3b helix, one helical turn apart. We propose that the 518 side chain does not interact with other channel domains, based on the observation that MTSES modification of 518C (increasing side chain volume) does not perturb channel function (Fig. 6A). Therefore, the face of the S3b helix, where positions 518 and 514 are located, is exposed to the extracellular aqueous phase, allowing interaction with APETx1. On the other hand, 517 and 519 side chains are likely to interact with other channel domains instead of being exposed to the extracellular aqueous phase, so that MTSET modification of 517C or 519C perturbs channel activation gating (Fig. 6A). Adding a positive charge at these two positions does not interfere with APETx1 binding. Therefore, this face of the S3b helix does not interact with APETx1.

The interaction surfaces of gating modifier toxins share the feature of having a hydrophobic patch surrounded by hydrophilic and charged residues (Wang et al., 2004; Swartz, 2007). There are differences in whether or how much the hydrophobic faces of these peptide toxins need to partition into the membrane lipid to access their binding sites, and the degree of toxin partitioning needs to match the S3–S4 linker length of the target channels. For example, site 4 peptide

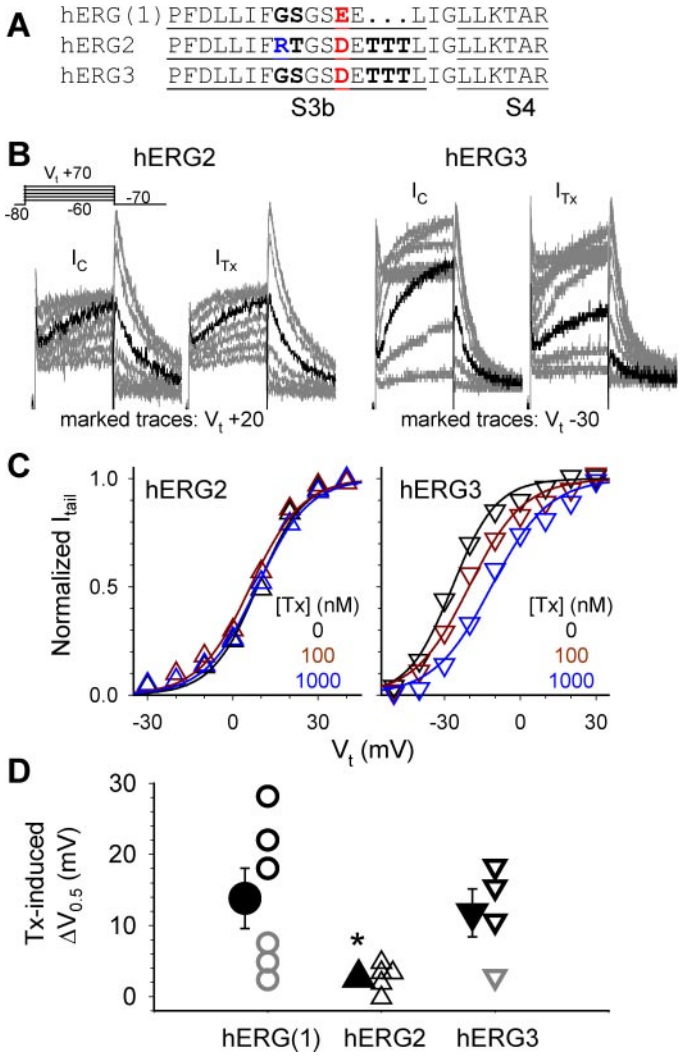

Fig. 7. Comparison of APETx1 effects on hERG isoforms. The WT hERG is marked as hERG(1). A, amino acid sequence alignment of the three hERG isoforms from S3b to the beginning of S4. Residues not conserved in all three isoforms are highlighted in boldface type. Accession numbers were the following: hERG2, Q9H252; and hERG3, Q9NS40. B, current traces from hERG2 and hERG3 recorded before and after adding 1 μM APETx1. The format is the same as in Fig. 3C, with V_t corresponding to $V_{0.5}$ under the control conditions. C, voltage-dependence of activation of hERG2 and hERG3 before and after adding 100 or 1000 nM APETx1. D, degree of $V_{0.5}$ shift caused by 1 μM APETx1. Open symbols denote data from individual oocytes, and solid symbols are mean with S.E. *, $p < 0.05$ of hERG2 versus hERG(1) or hERG3. $p > 0.05$ for hERG(1) versus hERG3.

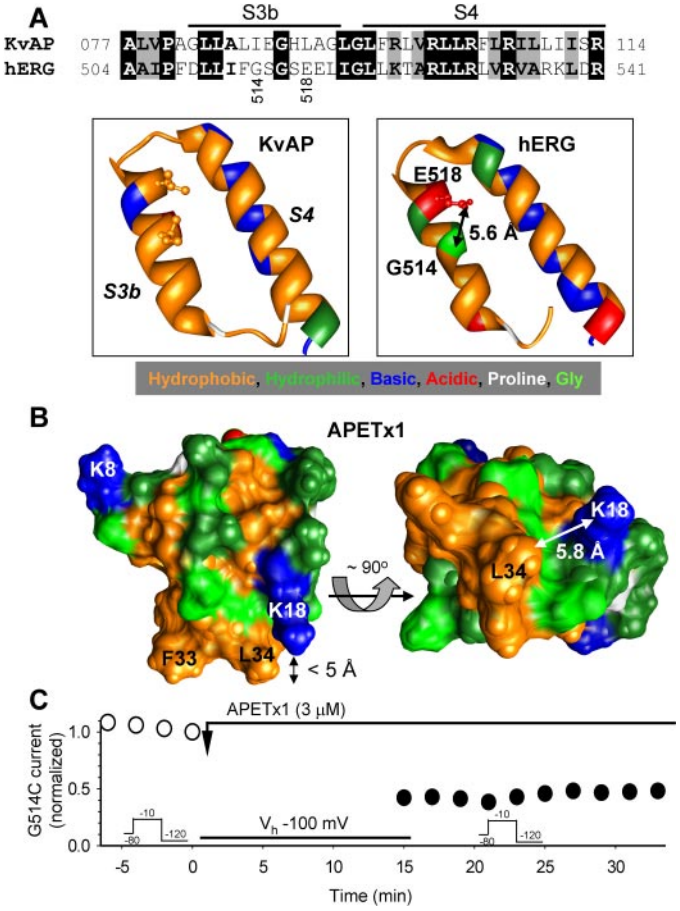

Fig. 8. A, top, amino acid sequence alignment between KvAP and hERG in the S3b-S4 region. Identical residues are highlighted by white lettering on black background, and similar residues are denoted by gray background. Bottom, three-dimensional structure of KvAP gating-paddle and a homology model of the corresponding region in hERG. Glu518 is shown in ball-and-stick format with distance between Gly514 (C_α) and Glu518 (C_δ) denoted. Color code for different types of side chains is listed below. B, side view (left) and front view (right) of APETx1 with surface rendered using the same color code as in A. Lys18, Lys8, Leu34, and Phe33 locations are labeled, and the distance between Lys18 (N_ε) and Leu34 (C_δ) is marked on the front view. C, test for state-dependence of APETx1 binding to the G514C mutant of hERG. Shown is the time course of change in G514C tail current amplitude elicited by voltage-clamp pulses diagrammed below the data points (applied once every 2 min). After stable control currents are recorded (○), pulsing is stopped, and the membrane is held at −100 mV for 15 min, during which APETx1 (3 μM) is added to the bath solution. Pulsing is resumed afterward, and data points are shown as ●.

toxins bind to the S3b region of domain II in the sodium channel, which has a relatively short S3–S4 linker (Swartz, 2007). Site 3 peptide toxins bind to the S3b region of domain IV in the sodium channel, which has a longer S3–S4 linker (Swartz, 2007). Experiments have suggested that site 4 peptide toxins partition into the membrane lipid, whereas site 3 peptide toxins do not (Smith et al., 2005). VSTx1 partitions into the membrane lipid to bind to KvAP's S3b, which has a very short S3–S4 linker (Fig. 8A) (Lee and MacKinnon, 2004). On the other hand, there seems to be a lesser degree of lipid partitioning for hanatoxin to bind to the S3b of Kv2.1, which has a relatively long S3–S4 linker (Phillips et al., 2005). The interaction surface of APETx1 has not been determined, but an inspection of its structure (Fig. 8B) and a comparison with the interaction surfaces of other gating modifier toxins suggest that Lys18 and Leu34/Phe33/Tyr32 are likely to be involved. In particular, the distance between Leu34 (C_δ) and Lys18 (N_ε) on APETx1 matches the predicted distance between Gly514 (C_α) and Glu518 (Cδ) on hERG's S3b (Fig. 8A). If Leu34, Phe33, and Tyr32 form a hydrophobic patch of the interaction surface, then the APETx1 has a short hydrophobic protrusion (<5 Å) and thus may not be able to partition deep into the membrane lipid.

Gating Paddle Movement During Activation in the hERG Channel. It has been shown that VSTx1 accesses its binding site on KvAP preferably at depolarized voltages (Jiang et al., 2003b). This is one of the arguments to support the proposal that KvAP's gating paddle moves from a location close to the intracellular side of the membrane to near the extracellular side during activation. Does hERG's gating paddle move a large distance during channel activation, similar to that proposed for the KvAP (Jiang et al., 2003b)? Another way to address this question is: can APETx1 access its binding site on hERG's S3b in the resting state? The experiment shown in Fig. 8C tests this possibility: applying APETx1 to the G514C mutant channel while holding the membrane at −100 mV does not prevent toxin effect; i.e., the toxin effect reaches its steady-state level at the first pulse after resuming the pulsing protocol. Similar observations are obtained in three other experiments: the effect of APETx1 10 μM reaches the steady-state level at the first pulse after adding the toxin (for only 2 min) while holding the membrane at −80 mV. These observations suggest that APETx1 can access its binding site in the resting state. Therefore, although the S3–S4 linker in the hERG channel is as short as that of the KvAP channel, hERG's gating paddle does not travel as much as that proposed for KvAP during activation. The face of hERG's S3b helix, where positions 518 and 514 are located, may face a water-filled crevice, allowing accessibility of APETx1 in the resting state of the channel.

MacKinnon and colleagues proposed a gating-paddle model for the movement of voltage-sensor during Kv channel activation based on the crystal structure and the state-dependence of avidin binding to biotin tethered to the voltage sensor of the KvAP channel (Jiang et al., 2003a,b). This model is supported by the lipid exposure of S4 based on an electron paramagnetic resonance study of KvAP in lipid bilayer (Cuello et al., 2004). However, this model is inconsistent with a large body of mutagenesis studies on eukaryotic Kv channels (Broomand et al., 2003; Gandhi et al., 2003; Lainé et al., 2003; Lee et al., 2003; Ahern and Horn, 2004; Starace and Bezanilla, 2004) and a more recent mammalian Kv1.2 crystal structure (Long et al., 2005). These observations raised questions about the relation between KvAP and eukaryotic Kv channels (Cohen et al., 2003). However, more recent crystallographic work showed that KvAP and Kv1.2 have similar structures and that the lipid membrane is required to maintain the correct orientations of transmembrane helices in KvAP (Lee et al., 2005). This is consistent with a study of channels in lipid bilayer using the luminescence-resonance energy transfer technique, which suggested that KvAP and Kv1.2 share a similar transmembrane helix arrangement, except that the voltage-sensor is closer to the pore domain in KvAP than in Kv1.2 (probably due to additional cytoplasmic domains in the eukaryotic channel) (Richardson et al., 2006).

References

Ahern CA and Horn R (2004) Specificity of charge-carrying residues in the voltage sensor of potassium channels. *J Gen Physiol* **123:**205–216.

Aiyar J, Withka JM, Rizzi J, Singleton DH, Andrews GC, Lin W, Boyd J, Hanson D, Simon M, Dethlefs B, et al. (1995) Topology of the pore-region of a K^+ channel revealed by the NMR-derived structures of scorpion toxins. *Neuron* **15:**1169–1181.

Bauer CK, Wulfsen I, Schafer R, Glassmeier G, Wimmers S, Flitsch J, Ludecke DK, and Schwarz JR (2003) HERG K^+ currents in human prolactin-secreting adenoma cells. *Pflugers Arch* **445:**589–600.

Broomand A, Mannikko R, Larsson HP, and Elinder F (2003) Molecular movement of the voltage sensor in a K channel. *J Gen Physiol* **122:**741–748.

Cestele S, Qu Y, Rogers JC, Rochat H, Scheuer T, and Catterall WA (1998) Voltage sensor-trapping: enhanced activation of sodium channels by β-scorpion toxin bound to the S3–S4 loop in domain II. *Neuron* **21:**919–931.

Chagot B, Diochot S, Pimentel C, Lazdunski M, and Darbon H (2005) Solution structure of APETx1 from the sea anemone *Anthopleura elegantissima*: a new fold for an HERG toxin. *Proteins* **59:**380–386.

Cohen BE, Grabe M, and Jan LY (2003) Answers and questions from the KvAP structures. *Neuron* **39:**395–400.

Corona M, Gurrola GB, Merino E, Cassulini RR, Valdez-Cruz NA, Garcia B, Ramirez-Dominguez ME, Coronas FIV, Zamudio FZ, Wanke E, et al. (2002) A large number of novel ergtoxin-like genes and ERG K^+-channel blocking peptides from scorpions of the genus *Centruroides*. *FEBS Lett* **532:**121–126.

Cuello LG, Cortes DM, and Perozo E (2004) Molecular architecture of the KvAP voltage-dependent K^+ channel in a lipid bilayer. *Science* **306:**491–495.

Diochot S, Loret E, Bruhn T, Beress L, and Lazdunski M (2003) APETx1, a new toxin from the sea anemone *Anthopleura elegantissima*, blocks voltage-gated human ether-a-go-go-related gene potassium channels. *Mol Pharmacol* **64:**59–69.

Fan J-S, Jiang M, Dun W, McDonald TV, and Tseng G-N (1999) Effects of outer mouth mutations on *hERG* channel function: a comparison with similar mutations in *Shaker*. *Biophys J* **76:**3128–3140.

Frenál K, Xu C-Q, Wolff N, Wecker K, Gurrola GB, Zhu S-Y, Chi C-W, Possani LD, Tytgat J, and Delepierre M (2004) Exploring structural features of the interaction between the scorpion toxin CnErg1 and ERG K^+ channels. *Proteins* **56:**367–375.

Gandhi CS, Clark E, Loots E, Pralle A, and Isacoff EY (2003) The orientation and molecular movement of a K^+ channel voltage-sensing domain. *Neuron* **40:**515–525.

Ganetzky B, Robertson GA, Wilson GF, Trudeau MC, and Titus SA (1999) The Eag family of K^+ channels in *Drosophila* and mammals. *Ann N Y Acad Sci* **868:**356–369.

Goldstein SAN, Pheasant DJ, and Miller C (1994) The charybdotoxin receptor of a *Shaker* K^+ channel: peptide and channel residues mediating molecular recognition. *Neuron* **12:**1377–1388.

Guex N and Peitsch MC (1997) Swiss-model and the Swiss-pdb Viewer: an environment for comparative protein modeling. *Electrophoresis* **18:**2714–2723.

Gurrola GB, Rosati B, Rocchetti M, Pimienta G, Zaza A, Arcangeli A, Olivotto M, Possani LD, and Wanke E (1999) A toxin to nervous, cardiac, and endocrine ERG K^+ channels isolated from *Centruroides noxius* scorpion venom. *FASEB J* **13:**953–962.

Hidalgo P and MacKinnon R (1995) Revealing the architecture of a K^+ channel pore through mutant cycles with a peptide inhibitor. *Science* **268:**307–310.

Hoffmann P and Warner B (2006) Are hERG channel inhibition and QT interval prolongation all there is in drug-induced torsadogenesis? A review of emerging trends. *J Pharmacol Toxicol Methods* **53:**87–105.

Huys I, Xu C-Q, Wang C-Z, Vacher H, Martin-Eauclaire M-F, Chi C-W, and Tytgat J (2004) BmTx3, a scorpion toxin with two putative functional faces separately active on A-type K^+ and HERG currents. *Biochem J* **378:**745–752.

Imredy JP and MacKinnon R (2000) Energetic and structural interactions between δ-dendrotoxin and a voltage-gated potassium channel. *J Mol Biol* **296:**1283–1294.

Jiang M, Zhang M, Maslennikov IV, Liu J, Wu DM, Korolkova YV, Arseniev AS, Grishin EV, and Tseng G-N (2005) Dynamic conformational changes of extracellular S5-P linkers in the hERG channel. *J Physiol* **569:**75–89.

Jiang Y, Lee A, Chen J, Ruta V, Cadene M, Chait BT, and MacKinnon R (2003a) X-ray structure of a voltage-dependent K^+ channel. *Nature* **423:**33–41.

Jiang Y, Ruta V, Chen J, Lee A, and MacKinnon R (2003b) The principle of gating charge movement in a voltage-dependent K^+ channel. *Nature* **423:**42–48.

Korolkova YV, Bocharov EV, Angelo K, Maslennikov IV, Grinenko OV, Lipkin AV, Nosireva ED, Pluzhnikov KA, Olesen S-P, Arseniev AS, et al. (2002) New binding site on the old molecular scaffold provides selectivity of HERG-specific scorpion toxin BeKm-1. *J Biol Chem* **277:**43104–43109.

Korolkova YV, Kozlov SA, Lipkin AV, Pluzhnikov KA, Hadley JK, Filippov AK, Brown DA, Angelo K, Strobaek D, Jespersen T, et al. (2001) An ERG channel inhibitor from the Scorpion *Buthus eupeus*. *J Biol Chem* **276:**9868–9876.

Laine M, Lin M-CA, Bannister JPA, Silverman WR, Mock AF, Roux B, and Papazian DM (2003) Atomic proximity between S4 segment and pore domain in Shaker potassium channels. *Neuron* **39:**467–481.

Lee HC, Wang JM, and Swartz KJ (2003) Interaction between extracellular hanatoxin and the resting conformation of the voltage-sensor paddle in Kv channels. *Neuron* **40:**527–536.

Lee SY and MacKinnon R (2004) A membrane-access mechanism of ion channel inhibition by voltage sensor toxins from spider venom. *Nature* **430:**232–235.

Lee S-Y, Lee A, Chen J, and MacKinnon R (2005) Structure of the KvAP voltage-dependent K^+ channel and its dependence on the lipid membrane. *Proc Natl Acad Sci U S A* **102:**15441–15446.

Li-Smerin Y and Swartz KJ (2000) Localization and molecular determinants of the hanatoxin receptors on the voltage-sensing domains of a K^+ channel. *J Gen Physiol* **115:**673–684.

Liu J, Zhang M, Jiang M, and Tseng G-N (2002) Structural and functional role of the extracellular S5-P linker in the HERG potassium channel. *J Gen Physiol* **120:**723–737.

Long SB, Campbell EB, and MacKinnon R (2005) Crystal structure of a mammalian voltage-dependent *Shaker* family K^+ channel. *Science* **309:**897–903.

Nastainczyk W, Meves H, and Watt DD (2002) A short-chain peptide toxin isolated from *Centruroides sculpturantus* scorpion venom inhibits *ether-a-go-go*-related gene K^+ channels. *Toxicon* **40:**1053–1058.

Pardo-López L, Garcia-Valdes J, Gurrola GB, Robertson GA, and Possani LD (2002a) Mapping the receptor site for ergtoxin, a specific blocker of ERG channels. *FEBS Lett* **510:**45–49.

Pardo-López L, Zhang M, Liu J, Jiang M, Possani LD, and Tseng G-N (2002b) Mapping the binding site of a HERG-specific peptide toxin (ErgTx) to the channel's outer vestibule. *J Biol Chem* **277:**16403–16411.

Pettersen EF, Goddard TD, Huang CC, Couch GS, Greenblatt DM, Meng EC, and Ferrin TE (2004) UCSF Chimera—a visualization system for exploratory research and analysis. *J Comput Chem* **25:**1605–1612.

Phillips LR, Milescu M, Li-Smerin Y, Mindell JA, Kim JI, and Swartz KJ (2005) Voltage-sensor activation with a tarantula toxin as cargo. *Nature* **436:**857–860.

Ranganathan R, Lewis JH, and MacKinnon R (1996) Spatial localization of the K^+ channel selectivity filter by mutant cycle-based structure analysis. *Neuron* **16:**131–139.

Rauer H, Lanigan MD, Pennington MW, Aiyar J, Ghanshani S, Cahalan MD, Norton RS, and Chandy KG (2000) Structure-guided transformation of charybdotoxin yields an analog that selectively targets Ca^{2+}-activated over voltage-gated K^+ channels. *J Biol Chem* **275:**1201–1208.

Restano-Cassulini R, Korolkova YV, Diochot S, Gurrola G, Guasti L, Possani LD, Lazdunski M, Grishin EV, Arcangeli A, and Wanke E (2006) Species diversity and peptide toxins blocking selectivity of ERG subfamily K^+ channels in CNS. *Mol Pharmacol* **69:**1673–1683.

Richardson J, Blunck R, Ge P, Selvin PR, Bezanilla F, Papazian DM, and Correa AM (2006) Distance measurements reveal a common topology of prokaryotic voltage-gated ion channels in the lipid bilayer. *Proc Natl Acad Sci U S A* **103:**15865–15870.

Rosati B, Marchetti P, Crociani O, Lecchi M, Lupi R, Arcangeli A, Olivotto M, and Wanke E (2000) Glucose- and arginine-induced insulin secretion by human pancreatic β-cells: the role of HERG K^+ channels in firing and release. *FASEB J* **14:**2601–2610.

Sanguinetti MC, Jiang C, Curran ME, and Keating MT (1995) A mechanistic link between an inherited and an acquired cardiac arrhythmia: HERG encodes the I_{Kr} potassium channel. *Cell* **81:**299–307.

Smith JJ, Alphy S, Seibert AL, and Blumenthal KM (2005) Differential phospholipid binding by site 3 and site 4 toxins. Implications for structural variability between voltage-sensitive sodium channel domains. *J Biol Chem* **280:**11127–11133.

Starace DM and Bezanilla F (2004) A proton pore in a potassium channel voltage sensor reveals a focused electric field. *Nature* **427:**548–553.

Swartz KJ (2007) Tarantula toxins interacting with voltage sensors in potassium channels. *Toxicon* **49:**213–230.

Tseng G-N (2001) I_{Kr}: the hERG channel. *J Mol Cell Cardiol* **33:**835–849.

Tseng G-N, Sonawane KD, Korolkova YV, Zhang M, Liu J, Grishin E, and Guy HR (2007) Probing outer mouth structure of the hERG channel with peptide toxin foot printing and molecular modeling. *Biophys J* **92:**3524–3540.

Wang J, Salata JJ, and Bennett PB (2003) Saxitoxin is a gating modifier of hERG K^+ channels. *J Gen Physiol* **121:**583–598.

Wang JM, Roh SH, Kim S, Lee CW, Kim JI, and Swartz KJ (2004) Molecular surface of tarantula toxins interacting with voltage sensors in K_v channels. *J Gen Physiol* **123:**455–467.

Winterfield JR and Swartz KJ (2000) A hot spot for the interaction of gating modifier toxins with voltage-dependent ion channels. *J Gen Physiol* **116:**637–644.

Zhang M, Korolkova YV, Liu J, Jiang M, Grishin EV, and Tseng G-N (2003) BeKm-1 is a hERG-specific toxin that shares the structure with ChTx but the mechanism of action with ErgTx1. *Biophys J* **84:**3022–3036.

Zhou W, Cayabyab FS, Pennefather PS, Schlichter LC, and DeCoursey TE (1998) HERG-like K^+ channels in microglia. *J Gen Physiol* **111:**781–794.

Address correspondence to: Dr. Gea-Ny Tseng, Department of Physiology, Medical College of Virginia, Virginia Commonwealth University, 1101 E. Marshall Street, Richmond, VA 23298. E-mail: gtseng@vcu.edu